

Direct observation of spin-quadrupolar excitations in $\text{Sr}_2\text{CoGe}_2\text{O}_7$ by high field ESR

Mitsuru Akaki,^{1,*} Daichi Yoshizawa,¹ Akira Okutani,¹ Takanori Kida,¹ Judit Romhányi,² Karlo Penc,^{3,4} and Masayuki Hagiwara¹

¹Center for Advanced High Magnetic Field Science,
Graduate School of Science, Osaka University, Toyonaka, 560-0043, Japan

²Okinawa Institute of Science and Technology Graduate University, Onna-son, Okinawa 904-0395, Japan

³Institute for Solid State Physics and Optics, Wigner Research Centre for Physics,
Hungarian Academy of Sciences, H-1525 Budapest, P.O.B. 49, Hungary

⁴MTA-BME Lendület Magneto-optical Spectroscopy Research Group, 1111 Budapest, Hungary

(Dated: September 11, 2022)

Exotic spin-multipolar ordering in large spin transition metal insulators has so far eluded unambiguous experimental observation. A less studied, but perhaps more feasible fingerprint of multipole character emerges in the excitation spectrum in the form of quadrupolar transitions. Such multipolar excitations are desirable as they can be manipulated with the use of light or electric field and can be captured by means of conventional experimental techniques. Here we study single crystals of multiferroic $\text{Sr}_2\text{CoGe}_2\text{O}_7$, and show that due to its nearly isotropic nature a purely quadrupolar bimagnon mode appears in the electron spin resonance (ESR) spectrum. This non-magnetic spin-excitation couples to the electric field of the light and becomes observable for a specific experimental configuration, in full agreement with a theoretical analysis of the selection rules.

Multipole moments formed by neighboring spins can simultaneously break time-reversal and spatial inversion symmetries, allowing for magneto-electric coupling and the mutual control of magnetization by electric and polarization by magnetic fields, providing new multiferroic materials for future technologies[1–4]. Well known examples are vector spin chirality and exchange striction driven electricity[5–7], both involving more than one spin.

Remarkably, in åkermanites – where CoO_4 tetrahedra form diagonal square lattices, alternating with intervening layers of alkaline earth metal ions along the c -axis (inset of Fig. 1) – the electric polarization is not induced by correlations between neighbouring spins, but is also present in the paramagnetic phase [8]. These compounds represent an exceptional family of magneto-electric materials, in which the finite (on-site) polarization emerges on the account of relativistic metal-ligand hybridization[9]. For this mechanism at least two conditions have to meet. The lack of inversion symmetry at Co sites permits magneto-electric coupling already for a single ion. Furthermore, the spin-3/2 magnetic moment of Co^{2+} allows for higher order multipole operators, such as the required quadrupole moment related to the emerging on-site polarization [9]. The metal-ligand hybridization is believed to act in $\text{Ba}_2\text{CoGe}_2\text{O}_7$ [10, 11], $\text{Sr}_2\text{CoSi}_2\text{O}_7$ [8], and $\text{Ca}_2\text{CoSi}_2\text{O}_7$ [12, 13].

When strong magnetic anisotropies are present, spin dipole and quadrupole degrees of freedom are usually mixed and it can be demanding to untangle the different types of multipolar fluctuations in the excitation spectrum. For example, $\text{Ba}_2\text{CoGe}_2\text{O}_7$ shows a large easy-plane magnetic anisotropy against a small exchange interaction. Correspondingly, the ‘electromagnon’, observed in its THz absorption spectrum, is of both dipolar

and quadrupolar character [14–16].

In this paper we study single crystals of $\text{Sr}_2\text{CoGe}_2\text{O}_7$ (SCGO) and show that its magnetic properties are uniquely isotropic in contrast to other members of its family. Due to the isotropic nature of SCGO, a precise classification of multipole excitations can be given. We use electron spin resonance technique in magnetic fields applied for different directions to show that a purely quadrupolar two-magnon mode exists in high magnetic fields. This excitation couples to specific components of polarization, and is not magnetically active. Our experimental findings are supported by theoretical analysis of the selection rules.

Figure 1 displays the magnetic field dependence of magnetization and electric polarization of SCGO at 1.4 K, below the Néel temperature of 6.5 K [17]. The magnetization in the ab -plane saturates at $3.42 \mu_B/\text{Co}$ just above 18 T, while along the c -axis the corresponding values are $3.3 \mu_B/\text{Co}$ and 21.6 T, leading to $g_{ab} = 2.28$ and $g_c = 2.2$. The magnetization curves are nearly isotropic, and the difference in the saturation fields is mainly explained by the g -tensor anisotropy. The magnetic anisotropy in SCGO is very small compared to that of $\text{Sr}_2\text{CoSi}_2\text{O}_7$ [8] or $\text{Ba}_2\text{CoGe}_2\text{O}_7$ [18]. The behavior of electric polarization as a function of magnetic field is nearly the same as in $\text{Sr}_2\text{CoSi}_2\text{O}_7$ [8]: it increases from zero with increasing magnetic field, and it is reversed at 16 T after reaching the maximum at about 7 T. This similarity suggests that the magnetic structure of SCGO is close to that of $\text{Sr}_2\text{CoSi}_2\text{O}_7$ and other Co åkermanite materials. According to previous neutron powder diffraction measurements [17], the spins lie in the ab -plane, the intra-plane coupling is antiferromagnetic, while the inter-plane coupling is weakly ferromagnetic.

Figure 2 shows the frequency-field plots of ESR res-

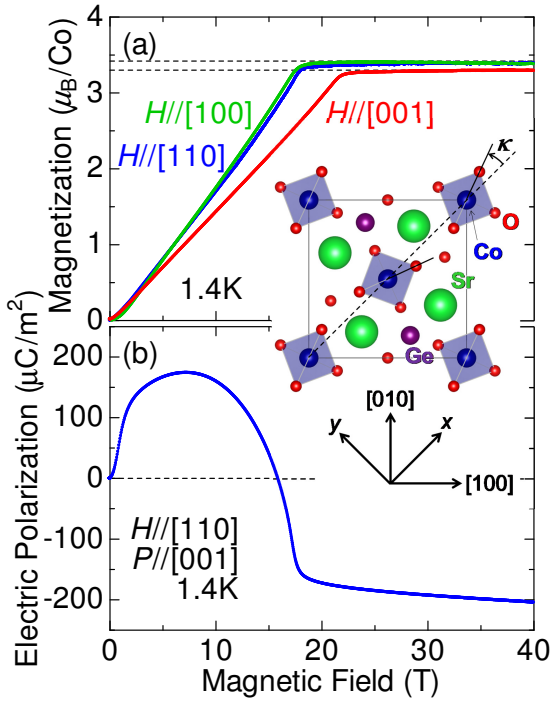


FIG. 1. Magnetic field dependence of (a) magnetization and (b) electric polarization of $\text{Sr}_2\text{CoGe}_2\text{O}_7$ at 1.4 K. The broken lines in (a) indicate the saturation magnetization values which are given by $g_{ab} = 2.28$ and $g_c = 2.2$. The inset shows the schematic crystal structure of $\text{Sr}_2\text{CoGe}_2\text{O}_7$ projected onto the ab -plane.

onance fields at 1.4–1.6 K. Three zero-field energy gaps are clearly identified: $\Delta_1 \approx 27$ GHz, $\Delta_2 \approx 220$ GHz, and $\Delta_3 \approx 700$ GHz. Gaps close to Δ_2 and Δ_3 were reported in THz spectroscopy measurements of $\text{Ba}_2\text{CoGe}_2\text{O}_7$ [14, 19], corresponding to transversal and longitudinal spin excitations, respectively. There, both Δ_2 and Δ_3 originate from the interplay of exchange and large single-ion easy-plane anisotropy [15, 19, 20]. The shape of the two lowest energy excitations clearly resembles the usual ESR spectra for the easy (ab) plane antiferromagnets [21]. The only difference is the existance of the smallest gap, Δ_1 , also observed in inelastic neutron diffraction measurements of $\text{Ba}_2\text{CoGe}_2\text{O}_7$ [22].

Next, we focus on the high-frequency Q_1 resonance mode in Fig. 2(a), observed above 20 T. It has a twice as large slope as the usual magnon, indicating absorption of two magnons. Figure 3 displays the ESR absorption spectra of SCGO at 1.4 K for Faraday geometry. The Q_1 bimagnon mode is visible for $H \parallel [100]$ only. The signal intensities of the D_1 mode show a negligible absorption for $H \parallel [100]$ and a strong absorption for $H \parallel [110]$. It appears that the absorption by the D_1 and Q_1 modes is mutually exclusive.

To further characterize the high field excitations, we compared the ESR spectra in Faraday ($\mathbf{H} \parallel \mathbf{k}$) and Voigt ($\mathbf{H} \perp \mathbf{k}$) geometries in Fig. 4. In the Faraday configura-

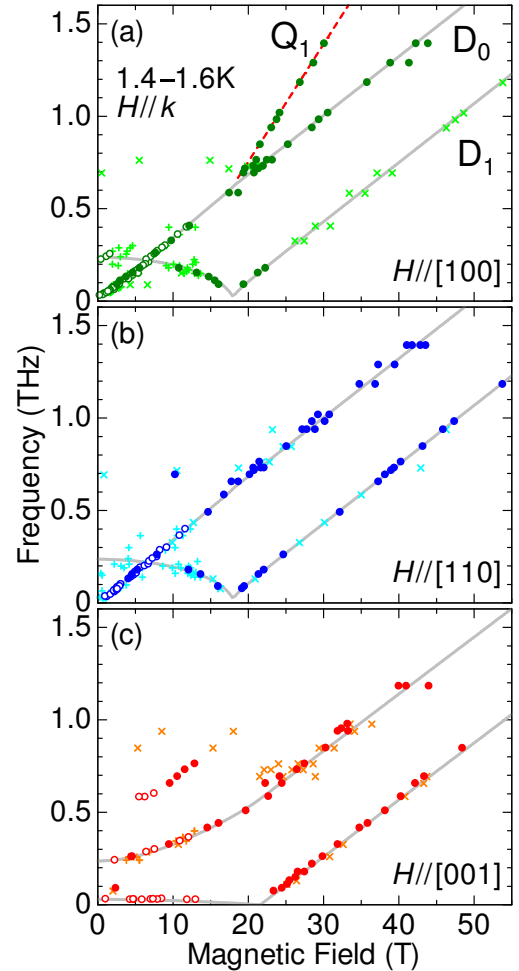


FIG. 2. Frequency-field diagrams of the ESR resonance fields of $\text{Sr}_2\text{CoGe}_2\text{O}_7$ for magnetic fields parallel to the (a) [100], (b) [110], and (c) [001] directions. Open circles (plus) are strong (weak) resonance signals obtained from the measurements in static fields at 1.6 K, while solid circles (cross) show strong (weak) resonance signals in pulsed fields at 1.4 K. The solid lines represent the resonance modes from the multiboson spin-wave theory. The broken line in (a) indicates a resonance mode with a slope twice larger than the others, corresponding to a two-magnon excitation.

tion, the field components of the incoming light are perpendicular to the direction of the static magnetic field and thus to the magnetic moments above saturation. Consequently, if a signal is present in the ESR spectrum, it is excited by components perpendicular to the static magnetic field. However, when a signal is missing in Faraday, but present in Voigt geometry, it is excited by the parallel component of the electromagnetic field. For example, in the case $\mathbf{H} \parallel [100]$, the D_1 magnon (open triangle in Fig. 4) is missing in the Faraday (dark green), but is present for the Voigt (light green) geometry. This means that only the [100] component of the light excites D_1 . The Q_1 bimagnon excitation (solid triangle in Fig. 4), present in the Faraday configuration, is coupled to [010]

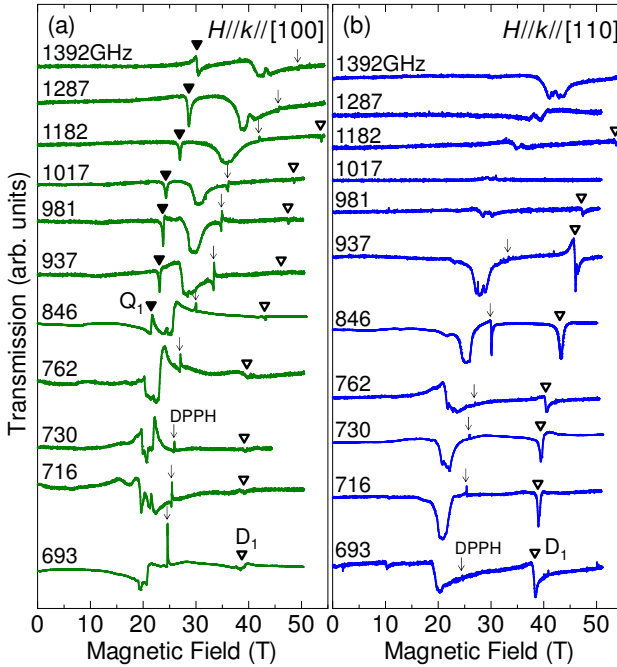


FIG. 3. Frequency dependent ESR absorption spectra of $\text{Sr}_2\text{CoGe}_2\text{O}_7$ in Faraday geometry at 1.4 K for (a) $\mathbf{H} \parallel [100]$ and (b) $\mathbf{H} \parallel [110]$. Arrows mark the resonance fields of DPPH (2,2-diphenyl-1-picrylhydrazyl, ESR marker with $g = 2.0036$). Open and solid triangles mark the resonance fields of one-magnon (D_1) and two-magnon (Q_1) resonance modes, respectively.

and/or [001] (since we used unpolarized light, we cannot separate the two components). Similarly, when $\mathbf{H} \parallel [110]$, the $[\bar{1}10]$ and/or [001] components of the oscillating fields excite the D_1 magnon, and the [110] component excites the Q_1 bimagnon.

We consider the following spin Hamiltonian as a minimal microscopic model for SCGO,

$$\mathcal{H} = J \sum_{\langle i,j \rangle} \mathbf{S}_i \cdot \mathbf{S}_j + J_{pz} \sum_{\langle i,j \rangle} P_i^z P_j^z + D \sum_i (S_i^z)^2 - \mu_B \sum_i [g_{ab}(H_x S_i^x + H_y S_i^y) + g_c H_z S_i^z], \quad (1)$$

where J is the exchange constant between the nearest neighbor spins, $D(>0)$ is the single ion anisotropy constant, and J_{pz} is the antiferroelectric constant. We neglect the Dzyaloshinskii-Moriya (DM) interactions and exchange anisotropies, which we found to be small (see supplement).

$$P_j^z = W_z \left\{ \cos 2\kappa \left[(\hat{S}_j^y)^2 - (\hat{S}_j^x)^2 \right] - (-1)^j \sin 2\kappa \overline{\hat{S}_j^x \hat{S}_j^y} \right\} \quad (2)$$

is the electric polarization operator originating from $p-d$ hybridization, with similar expressions for P_j^x and P_j^y

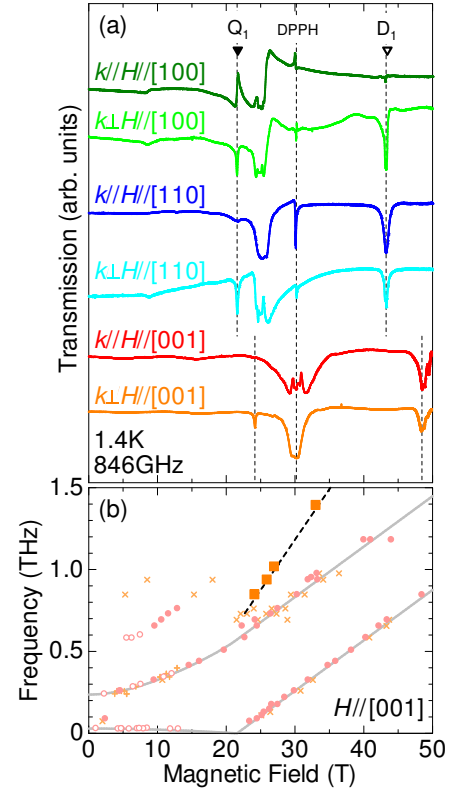


FIG. 4. (a) ESR absorption spectra of $\text{Sr}_2\text{CoGe}_2\text{O}_7$ at 846 GHz in Faraday ($\mathbf{k} \parallel \mathbf{H}$) and Voigt ($\mathbf{k} \perp \mathbf{H}$) geometry for $\mathbf{H} \parallel [100]$, $\mathbf{H} \parallel [110]$, and $\mathbf{H} \parallel [001]$. Vertical dotted lines, from left to right, indicate two-magnon resonance signal, signal of ESR standard DPPH, and one-magnon resonance signal, respectively. (b) Frequency-field diagrams of the ESR resonance fields in the Voigt-geometry for $\mathbf{H} \parallel [001]$ directions, showing the two-magnon absorptions (orange squares).

[11], where $\overline{UV} = UV + VU$. The parity of the site index j differs for the two sublattices, so that the $(-1)^j$ accounts for alternation of the rotation angles $\kappa \approx \pm 20.5^\circ$ of the CoO_4 tetrahedra from the [110] direction (inset of Fig. 1) [17]. Note the spin quadrupole operators in Eq. (2), which may excite bimagnons (Q) – this is in contrast with the spin-current mechanism, where the magnetoelectric coupling involves a bilinear, but spin-dipole operator only.

Without the J_{pz} term the Hamiltonian represents an easy plane antiferromagnet with a Goldstone mode ($\Delta_1 = 0$). A finite J_{pz} was introduced for $\text{Ba}_2\text{CoGe}_2\text{O}_7$ to explain the vanishing of electric polarization in zero field [23] and the absence of Goldstone modes in the neutron scattering study [22]. At zero magnetic field, the electric polarization is also zero in SCGO (Fig. 1(b)), hence the ground state must be an antiferroelectric state, selecting [100] as the magnetic easy axis within the easy plane.

To understand the physics at high magnetic fields in simple terms, we start from the fully saturated state,

\mathbf{H}	$P_{(0,0)}^{\parallel}$	$P_{(\pi,\pi)}^{\parallel}$	$\perp (1)$	$P_{(0,0)}^{\perp(1)}$	$P_{(\pi,\pi)}^{\perp(1)}$	$\perp (2)$	$P_{(0,0)}^{\perp(2)}$	$P_{(\pi,\pi)}^{\perp(2)}$
$H \parallel [100]$	(Q_0)	D_1	$[010]$	D_0	Q_1	$[001]$	D_0	Q_1
$H \parallel [110]$	D_0	Q_1	$[\bar{1}10]$	(Q_0)	D_1	$[001]$	(Q_0)	D_1
$H \parallel [001]$	(Q_0)	Q_1	$[100]$	D_0	D_1	$[010]$	D_0	D_1

TABLE I. The branches in the ESR spectrum the uniform $P_{(0,0)}$ and staggered $P_{(\pi,\pi)}$ components of the polarization excite. The electric field which couples to P^{\parallel} is present in Voigt geometry only, while the perpendicular components P^{\perp} are also present in Faraday geometry. The Q_0 quadrupolar excitations are silent in the experiment.

where all the spins are parallel to the field with $S^{\parallel} = 3/2$ – we choose the direction of the field as the quantization axis, along which the spin operator $S^{\parallel} = \mathbf{S} \cdot \mathbf{H}/H$ is diagonal. A single magnon excitation corresponds to lowering the S^{\parallel} spin component from $3/2$ to $1/2$ on a single site, which propagates due to the off diagonal terms in the exchange interaction. The spin Hamiltonian (1) is translationally invariant with a single spin per unit cell, and we end up with a cosine like dispersion in the extended Brillouin zone of the square lattice. The magnon dispersion at $\mathbf{q} = (0, 0)$ gives the paramagnetic signal D_0 , slightly shifted by anisotropies,

$$\omega_{D_0} = \begin{cases} \mu_B g_c H - 2D, & \text{if } \mathbf{H} \parallel [001], \\ \mu_B g_{ab} H + D + \dots, & \text{if } \mathbf{H} \perp [001]. \end{cases} \quad (3)$$

As the $\sum_i S_i^z$ commutes with the Hamiltonian (1), the above expression is exact for $\mathbf{H} \parallel [001]$. We used perturbation theory to calculate the asymptotic expression for ω_{D_0} when $\mathbf{H} \perp [001] \gg D, J$ (also for ω_{D_1} and ω_{Q_1} below, see supplementing material for details). Since J is anti-ferromagnetic, the magnon dispersion has a minimum at $\mathbf{q} = (\pi, \pi)$, providing the energies of the D_1 modes,

$$\omega_{D_1} = \begin{cases} \mu_B g_c H - 12J - 2D, & \text{if } \mathbf{H} \parallel [001], \\ \mu_B g_{ab} H - 12J + D + \dots, & \text{if } \mathbf{H} \perp [001]. \end{cases} \quad (4)$$

A linear fit to the ω_{D_1} for large $H \parallel [100]$ and $[110]$ shown in Fig. 2(a) and (b) gives an $\omega_{D_1} = 0$ intercept at 16.5 T, while for $H \parallel [001]$ the intercept coincides with the saturation field, 21.6 T. From Eqs. (4), the estimated values of magnetic exchange interaction and easy-plane anisotropy are $J = 2.29$ K and $D = 2.2$ K. This result is also consistent with the measured shift between the two single-magnon modes, $\omega_{D_0} - \omega_{D_1} = 12J \approx 600$ GHZ. The ratio $D/J = 0.96$, and therefore the reduction of spin length in the mean field theory, is much smaller in SCGO than in $\text{Ba}_2\text{CoGe}_2\text{O}_7$ [15, 19]. As a consequence, the dipole and quadrupole characters of the different modes are well separated here. To test our parameters, we calculated the the single-magnon modes D_0 and D_1 from the multiboson spin-wave theory[24]. Adding a

small $W_z^2 J_{pz}/k_B = 2.5 \times 10^{-5}$ K, the calculated and the measured modes show an excellent agreement, even in the low field regime, as shown in Fig. 2.

The D_1 magnon mode is usually not observed in the ESR spectra, unless DM interaction is present [25]. In SCGO, however, the staggered component of the polarization can interact with the electric field of the light, leading to absorption at $\mathbf{q} = (\pi, \pi)$. Indeed, when $\mathbf{H} \parallel [110]$ and the spins point along the x direction ($S^{\parallel} \equiv S^x$), the staggered component of the \hat{P}_j^z in Eq. (2) creates a (π, π) magnon, giving rise to the D_1 branch in Fig. 2. For $\mathbf{H} \parallel [100]$, the spin quadrupole operator in the staggered component of \hat{P}_j^z creates an $S^{\parallel} = -1/2$ state with $\mathbf{q} = (\pi, \pi)$ and energy

$$\omega_{Q_1} = \begin{cases} 2\mu_B g_c H - 12J - 2D, & \text{if } \mathbf{H} \parallel [001], \\ 2\mu_B g_{ab} H - 12J + D + \dots, & \text{if } \mathbf{H} \perp [001], \end{cases} \quad (5)$$

leading to the Q_1 resonance mode. Although multipole fluctuations have long been theoretically proposed[26–29], the Q_1 mode in the saturated state of SCGO is, up to our knowledge, the first unambiguous experimental observation of a purely quadrupole excitation in a quantum magnet.

The difference between the dipolar and quadrupolar modes is illustrated in Fig. 5. In the D_1 dipolar mode, the expectation value of the spin operators (shown by a green arrow)

$$\begin{aligned} \langle S^{[\bar{1}10]} \rangle &\propto \sin(\omega_{D_1} t + \phi_j), \\ \langle S_j^{[001]} \rangle &\propto \cos(\omega_{D_1} t + \phi_j), \\ \langle S_j^{[100]} \rangle &\approx \frac{3}{2}, \end{aligned} \quad (6)$$

describes a precession around the static component of the spin. In the quadrupolar modes, the quadrupolar moments (shown by a green ellipse)

$$\begin{aligned} \overline{\langle S_j^{[001]} S_j^{[010]} \rangle} &\propto \sin(\omega_{Q_1} t + \phi_j), \\ \langle (S_j^{[001]})^2 - (S_j^{[010]})^2 \rangle &\propto \cos(\omega_{Q_1} t + \phi_j), \end{aligned} \quad (7)$$

rotate around the static spin component. The $\phi_j = j\pi$ phase ensures the $\mathbf{q} = (\pi, \pi)$ wave vector of the excitations.

The different transitions are collected in Tab. I. It turns out, that the uniform components of the polarizations can also create quadrupole excitations at $\mathbf{q} = (0, 0)$, but they are not seen in the experiment. The resolution of this puzzle lies in the structure of the two-magnon excitation spectrum. Two $S^{\parallel} = 1/2$ magnons give rise to a two-magnon continuum. Owing to the cosine-like dispersion, this continuum is the broadest at $\mathbf{q} = (0, 0)$, extending from $2\omega_{D_1}$ to $2\omega_{D_0}$, and it shrinks to a single point at $\mathbf{q} = (\pi, \pi)$ with energy $\omega_{D_0} + \omega_{D_1} \neq \omega_{Q_1}$. The $S^{\parallel} = -1/2$ state at $\mathbf{q} = (\pi, \pi)$ is decoupled from the

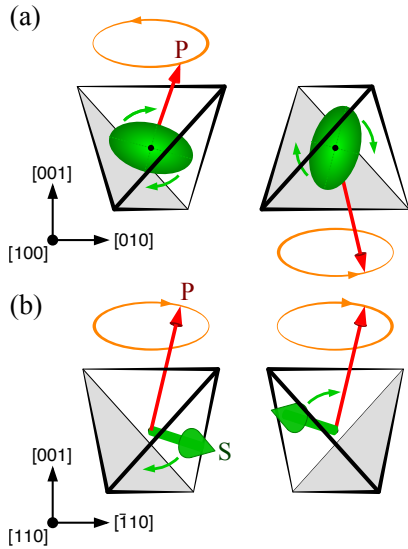


FIG. 5. Schematic plot of the (a) quadrupolar mode Q_1 for $\mathbf{H} \parallel [100]$ and (b) the dipolar wave D_1 for $\mathbf{H} \parallel [110]$, as seen from the direction of the magnetic field. The green ellipse represents the rotating quadrupolar moments, while the green arrows the precessing dipolar spin. The red arrows show the electric polarization vector.

two-magnon continuum [30], resulting in a sharp absorption peak at ω_{Q_1} . However, the Q_0 quadrupole mode, at $\mathbf{q} = (0, 0)$, interacts with two $S^{\parallel} = 1/2$ magnons deep inside the continuum and decays very quickly, making it unobservable (see supplementing material).

In conclusion, we studied multipole excitations in single crystals of the magnetoelectric insulator, SCGO. Bimagnon modes have already been observed in the excitation spectrum of the other åkermanites[19], as well as in the spin-1 chain compound, $\text{NiCl}_2\text{-}4\text{SC}(\text{NH}_2)_2$ [31]. However, in those materials the single-ion anisotropy is the dominant term, reducing the spin length considerably and mixing the dipolar and quadrupolar degrees of freedom. As a result, magnon and bimagnon modes have both dipolar and quadrupolar character, and couple to magnetic and electric components of the exciting light in earlier experiments.

The nearly isotropic property of SCGO, on the other hand, allows for the emergence of uniquely pure quadrupolar excitations, appearing completely detached from magnetic transitions. Using multifrequency ESR technique, supported by theoretical investigation of transition matrix elements, we clarified the quadrupolar nature of the bimagnon excitation. Furthermore, based on analytical description of the excitations, available in the high field regime, and utilizing the measured saturation fields, we calculated the magnetic coupling values, as well as the components of the g -tensor. The spin wave spectrum with the evaluated parameter values is in excellent agreement with the measurements, throughout the entire magnetic field regime and for each field direction.

Our investigations can serve as basis for further studies of emerging multipolar excitations with the use of well-spread experimental approaches, such as the ESR in the present work. Detecting such modes could help designing new magnetoelectric devices, in which electrically active magnetic excitations may carry and store information. Furthermore, it may serve as a guide in the quest for nematic and more exotic, otherwise undetectable ‘hidden’ orders.

Methods

Single crystalline samples of SCGO were grown by the floating zone method. X-ray diffraction measurements confirmed the tetragonal $P\bar{4}2_1m$ structure with no impurity phases. The magnetization was measured in pulsed fields of up to 55 T and the magnetic field induced electric polarization was obtained by integrating the polarization current. Low-field ESR spectra up to 14 T were taken using a home-made transmission ESR cryostat in a superconducting magnet. High-field ESR measurements at 1.4 K in pulsed magnetic fields of up to 55 T were conducted by utilizing a far-infrared laser and Gunn oscillators coupled with a frequency doubler to generate submillimeter and millimeter waves, and InSb bolometer as a detector.

The dispersions were calculated using perturbation expansion in D above the saturation field for $\mathbf{H} \perp [001]$. In addition, we used a multiboson spin-wave theory to calculate the excitation spectrum.

* akaki@ahmf.sci.osaka-u.ac.jp

- [1] T. Kimura, T. Goto, H. Shintani, K. Ishizaka, T. Arima, and Y. Tokura, *Nature (London)* **426**, 55 (2003).
- [2] M. Fiebig, *J. Phys. D* **38** R123 (2005).
- [3] Y. Tokura, S. Seki and N. Nagaosa, *Rep. Prog. Phys.* **77** 076501 (2014).
- [4] T. Arima, *J. Phys. Soc. Jpn.* **80** 052001 (2011).
- [5] H. Katsura, N. Nagaosa, and A. V. Balatsky, *Phys. Rev. Lett.* **95**, 057205 (2005).
- [6] I. A. Sergienko and E. Dagotto, *Phys. Rev. B* **73**, 094434 (2006).
- [7] C. Jia, S. Onoda, N. Nagaosa, and J. H. Han, *Phys. Rev. B* **76**, 144424 (2007).
- [8] M. Akaki, H. Iwamoto, T. Kihara, M. Tokunaga, and H. Kuwahara, *Phys. Rev. B* **86**, 060413(R) (2012).
- [9] T. Arima, *J. Phys. Soc. Jpn.* **76**, 073702 (2007).
- [10] H. Y. Yi, Y. J. Choi, S. Lee, and S.-W. Cheong, *Appl. Phys. Lett.* **92**, 212904 (2008).
- [11] H. Murakawa, Y. Onose, S. Miyahara, N. Furukawa, and Y. Tokura, *Phys. Rev. Lett.* **105**, 137202 (2010).
- [12] M. Akaki, J. Tozawa, D. Akahishi, and H. Kuwahara, *Appl. Phys. Lett.* **94**, 212904 (2009).
- [13] M. Akaki, H. Kuwahara, A. Matsuo, K. Kindo, and M. Tokunaga, *J. Phys. Soc. Jpn.* **83**, 093704 (2014).

- [14] I. Kézsmárki, N. Kida, H. Murakawa, S. Bordács, Y. Onose, and Y. Tokura, *Phys. Phys. Lett.* **106**, 057403 (2011).
- [15] S. Miyahara and N. Furukawa, *J. Phys. Soc. Jpn.* **80**, 073708 (2011).
- [16] I. Kézsmárki, D. Szaller, S. Bordács, V. Kocsis, Y. Tokunaga, Y. Taguchi, H. Murakawa, Y. Tokura, H. Engelkamp, T. Rööm, and U. Nagel, *Nature Communications* **5**, 3203 (2014).
- [17] T. Endo, Y. Doi, Y. Hinatsu, and K. Ohoyama, *Inorg. Chem.* **51**, 3572-3578 (2012).
- [18] V. Hutana, A. P. Sazonov, M. Meven, G. Roth, A. Gukasov, H. Murakawa, Y. Tokura, D. Szaller, S. Bordács, I. Kézsmárki, V. K. Guduru, L. C. J. M. Peters, U. Zeitler, J. Romhányi, and B. Náfrádi, *Phys. Rev. B* **89**, 064403 (2014).
- [19] K. Penc, J. Romhányi, T. Rööm, U. Nagel, Á. Antal, T. Fehér, A. Jánossy, H. Engelkamp, H. Murakawa, Y. Tokura, D. Szaller, S. Bordács, and I. Kézsmárki, *Phys. Rev. Lett.* **108**, 257203 (2012).
- [20] M. Matsumoto and M. Koga, *J. Phys. Soc. Jpn.* **76**, 073709 (2007).
- [21] T. Nagamiya, K. Yosida, and R. Kubo, *Advances in Physics* **4**, 1 (1955).
- [22] M. Soda, M. Matsumoto, M. Måansson, S. Ohira-Kawamura, K. Nakajima, R. Shiina, and T. Masuda, *Phys. Rev. Lett.* **112** 127205 (2014).
- [23] J. Romhányi, M. Lajkó, and K. Penc, *Phys. Rev. B* **84**, 224419 (2011).
- [24] J. Romhányi and K. Penc, *Phys. Rev. B* **86**, 174428 (2012).
- [25] S. A. Zvyagin, D. Kamenskyi, M. Ozerov, J. Wosnitza, M. Ikeda, T. Fujita, M. Hagiwara, A. I. Smirnov, T. A. Soldatov, A. Ya. Shapiro, J. Krzystek, R. Hu, H. Ryu, C. Petrovic, and M. E. Zhitomirsky, *Phys. Rev. Lett.* **112**, 077206 (2014).
- [26] A. V. Chubukov, *J. Phys.: Condens. Matter* **2** (1990).
- [27] F. P. Onufrieva, *Physica B* **186-188** 837-840 (1993).
- [28] R. Shiina, H. Shiba, P. Thalmeier, A. Takahashi and O. Sakai, *J. Phys. Soc. Jpn.* **72**, 1216 (2003).
- [29] M. Matsumoto, *J. Phys. Soc. Jpn.* **83**, 084704 (2014).
- [30] R. Silbergliit and J. B. Torrance, Jr., *Phys. Rev. B* **2**, 772 (1970).
- [31] S. A. Zvyagin, J. Wosnitza, C. D. Batista, M. Tsukamoto, N. Kawashima, J. Krzystek, V. S. Zapf, M. Jaime, N. F. Oliveira, Jr., and A. Paduan-Filho, *Phys. Rev. Lett.* **98**, 047205 (2007).

Acknowledgements

We thank K. Yamauchi and T. Oguchi for helpful discussions. This work was supported in part by the Grants-in-Aid for Scientific Research (Grant Nos. 15K05145, 25220803, 24244059, and 25246006) from MEXT, Japan and by JSPS Core-to-Core Program, A Advanced Research Networks and by the Hungarian OTKA Grant No. K106047.

Author contributions

M.A. planned and performed the experiments in collaboration with D.Y., A.O., T.K., and M.H. Single crystals of SCGO were grown and prepared for experiments by M.A. M.A. and T.K. performed high-field magnetization and electric polarization measurements. M.A., D.Y. and A.O. performed ESR measurements. M.A. and M.H. analyzed the data. Theoretical calculations were done by J.R. and K.P. All authors discussed the results.